Lehrstuhl für Bildverarbeitung
Institute of Imaging & Computer Vision

Comparative Analysis of Shift Variance and Cyclostationarity in Multirate Filterbanks

Til Aach

Institute of Imaging and Computer Vision
RWTH Aachen University, 52056 Aachen, Germany
tel: +49 241 80 27860, fax: +49 241 80 22200
web: www.lfb.rwth-aachen.de

in: IEEE Transactions on Circuits and Systems –I: Regular Papers. See also BIBTEX entry below.

BIBTEX:

```
@article{AAC07a,
author = {Til Aach},
title = {Comparative Analysis of Shift Variance and Cyclostationarity in Multirate
                        Filterbanks},
journal = {IEEE Transactions on Circuits and Systems {--I}: {R}egular Papers},
publisher = {IEEE},
volume = {54},
number = {5},
year = {2007},
pages = {1077--1087}}
```


document created on: June 1, 2007
created from file: fbankscascover.tex
cover page automatically created with CoverPage.sty
(available at your favourite CTAN mirror)

Comparative Analysis of Shift Variance and Cyclostationarity in Multirate Filter Banks

Til Aach, *Senior Member, IEEE*

***Abstract*— Multirate filter banks introduce periodic time-varying phenomena into their subband signals. The nature of these effects depends on whether the signals are regarded as deterministic or as random signals. We analyze the behavior of deterministic and wide-sense stationary (WSS) random signals in multirate filter banks in a comparative manner. While aliasing in the decimation stage causes subband energy spectra of deterministic signals to become shift-variant, imaging in the interpolation stage causes WSS random signals to become WS cyclostationary (WSCS). We provide criteria to quantify both shift variance and cyclic nonstationarity. For shift variance, these criteria separately assess the shift dependence of energy and of energy spectra. Similarly for nonstationarity, they separately assess the nonstationary behavior of signal power and of power spectra. We show that, under aliasing cancellation and perfect reconstruction constraints of paraunitary and biorthogonal filter banks, these criteria evaluate the behavior of deterministic and WSS random signals in a consistent, dual way. We apply our criteria to paraunitary and biorthogonal filter banks as well as to orthogonal block transforms, and show that, for critical signals such as lines or edges in image data, the biorthogonal 9/7 filters perform best among these.**

***Index Terms*— Multirate filters, decimation, interpolation, cyclic nonstationarity, paraunitary filter banks, biorthogonal filter banks.**

I. Introduction

CONVERSION of sampling rates in multirate filter systems [1], [2] generally introduces periodic shift variance in the sense that when a given, deterministic input signal is shifted in time or space, its subband coefficients do not translate correspondingly. Instead, subband energy may be redistributed significantly between subbands [3]. The outcome of lossy subband compression [4], [5], [6] or of nonlinear adaptive subband processing for, say, X-ray image enhancement [7], thus depends on translations of the input data. Analysis and assessment of the shift-variant behavior of the subbands of deterministic signals are hence important issues. Loeffler and Burrus [8] describe multirate filters via linear periodically time-varying (LPTV) systems, and employ two-dimensional spectral representations — referred to as bifrequency maps [2] — to describe the LPTV properties. In particular, they show that the shift-invariant and shift-variant parts of an LPTV filter are separated in the bifrequency map, and point out that its time-varying behavior can thus be determined from the off-diagonal components of the bifrequency map. Similarly, Vaidyanathan and Mitra show that LPTV systems can be represented by critically sampled polyphase networks [9]. Simoncelli et. al. [3] show that, as a consequence of aliasing in the analysis stage, the subband energy of a decimated deterministic signal generally oscillates when the signal is shifted in time. Complementing these frequency-domain descriptions, Villasenor et. al. [4] provide a time-domain analysis of the periodic shift variance in terms of the time-variant impulse response of wavelet filter banks when only the low-frequency signal (or reference signal) is retained. They show that the time-variant impulse response of the lowpass channel of a dyadic wavelet transform can be written as a weighted linear combination of the upsampled versions of the synthesis lowpass [4, Eq. (12)]. The weights are taken from shift-dependent subsets of the analysis filter coefficients, a view which is consistent with the above result that shift variance is generated by aliasing in the analysis filter bank. Furthermore, [4] identifies a selection of biorthogonal filter banks best suited for image compression, without, though, defining a quantitative measure for shift variance.

Approaches to shift-invariant wavelet respresentations include, e.g., normalization of signals with respect to position and width in time [10], [11], operating without sampling rate conversion [12] and cycle spinning [13]. In cycle spinning, several circularly translated versions of a given input signal are processed independently. The processing results are then shifted back and averaged, yielding the final translation-invariant result. Liang and Parks [14] calculate the wavelet decomposition for all circular shifts of the input signal, and select the best representation via a binary tree search. Another approach is the use of complex wavelets [15], [16], which, when applied to two-dimensional images, also provide better directional selectivity than real-valued separable wavelets [17], [18], [19], [20]. A genetic algorithm to optimize wavelet filters with respect to shift invariance can be found in [21].

In applications such as lossy image compression [5], [6], [20] or filter approximation [22], performance is assessed by the *expected* error, often on the basis of wide-sense stationary (WSS) signal models. Since the statistical properties of stationary random signals do, by definition, not depend on time shifts, the concept of shift variance cannot be applied. A WSS random signal, however, does generally not remain stationary when passing through a multirate filter bank branch. Rather, the correlation structure and power spectra at the output of a filter bank branch vary periodically, thus making the output process wide sense cyclostationary (WSCS) [23], [24], [25],

T. Aach is with the Institute of Imaging and Computer Vision, RWTH Aachen University, D-52056 Aachen, Germany.

Parts of this work were published at the 6th IEEE Nordic Signal Processing Symposium (NORSIG), Espoo, June 9-11 2004, and at the International Workshops on Spectral Methods and Multirate Signal Processing (SMMSP) in Florence, Sept. 1-3, 2006, Vienna, Sept. 11-12, 2004, and Barcelona, Sept. 13-14, 2003.

[26], [27], [28], [29], [30], [31]. Performance measures such as mean square error or the nonaliasing energy ratio (NER) [32] average over the periodical variations, thus implicitly assuming a WSS signal. In [23], Sathe and Vaidyanathan analyze WSCS signals with period L in terms of L-dimensional vector random signals, where the vectors are formed from L successive coefficients of the original scalar signal. While this vector signal is WSS, the original signal is WSS if the power spectrum matrix of the vector process is a pseudocirculant matrix. Similarly, they relate LPTV systems to linear time-invariant (LTI) multiple-input multiple output (MIMO) systems, and show that, if the transfer matrix of the LTI-MIMO system is pseudocirculant [9], the scalar filter is LTI rather than LPTV. They prove that decimation in the analysis filter bank keeps a WSS signal WSS, and may even turn a WSCS signal into a WSS signal (see also [25], [27], [28], [29], [33], [34]). Vice versa, interpolation in the synthesis bank transforms a WSS signal into a WSCS signal unless an ideal anti-imaging filter is used. A later paper [31] arrives at these conclusions using bifrequency maps as in [2], [8]. In [25], [26], [27], the power spectral matrix of an interpolator is derived. As in [8] for LPTV systems, the cyclic nonstationary part of the output signal is determined by its off-diagonal entries, while the diagonal determines the stationary part. A comprehensive list of references on cyclostationarity and multirate filter banks can be found in sections 2.6.1 and 3.6.8 of the bibliography by Serpedin et. al. [35].

The objective of this paper is to quantify the shift-variant and cyclic nonstationary behavior of various multirate filter banks in a parallel, comparative manner. From a separation of the shift-invariant and shift-variant parts of the subband energy spectra of a deterministic signal as well as of the WSS and nonstationary parts of the WSCS subband power spectra of a WSS random input signal, we develop quantitative criteria to evaluate shift variance and cyclic nonstationarity in a multirate filter bank. Inserting aliasing cancellation conditions and perfect reconstruction (PR) constraints of paraunitary and biorthogonal filter banks, we derive a duality between the behavior of deterministic and WSS random signals with flat spectra. Based on these criteria, we compare a variety of paraunitary and biorthogonal filter banks as well as several orthogonal block transforms. Our comparison is carried out for standard input signals, such as first order autogressive random signals, as well as for signals where, e.g., shift variance is most critical, such as lines or edges in image data.

In a multirate PR filter bank, the aliasing terms at its channel outputs cancel at the filter bank output provided the subbands are not processed. Subband processing by, for instance, quantization, compression or filtering, distorts the balance between the aliasing terms, and thus lets effects such as shift variance appear in the filter bank output signal. These then depend on the properties of both the filter bank and the type of processing. In general for the filter banks which are of interest here, it is safe to assume that, for a given type of subband processing, shift variance in the output signal is low when shift variance in each filter bank channel is low. In other words, for a filter bank with low shift variance in each channel, a higher degree of subband processing will be permitted (cf. also the discussion on aliasing cancellation in [15]). Fig. 1 shows a channel of a multirate filter bank, consisting of a downsampler followed by an upsampler placed between analysis and synthesis filters $H(z)$ and $G(z)$. The input signal is denoted by $s(n)$. In the deterministic case, it is assumed to be of finite energy with z-transform $S(z)$ and energy spectrum $R^E_{ss}(z) = S(z)S(z^{-1})$. In the WSS case, its autocorrelation sequence (ACS) is $r_{ss}(n) = E[s(m)s(m+n)]$, where E is the expectation operator. The z-transform of $r_{ss}(n)$ is the power spectrum $R_{ss}(z)$. The signals within the filter bank channel are denoted as indicated in Fig. 1: $t(n)$ is the analysis-filtered signal, $x(n)$ the downsampled signal, $v(n)$ the signal after upsampling, and $y(n)$ the channel output. The Mth root of one is denoted by $e^{-j2\pi/M} = W$, and the Fourier matrix by $\mathbf{W}$. The modulation vector of a signal $s(n)$ is denoted by $\mathbf{s}_m(z) = [S(z), S(zW), \ldots, S(zW^{M-1})]^T$. The modulation vectors of the filters $h(n)$ and $g(n)$ are denoted by $\mathbf{h}_m(z)$ and $\mathbf{g}_m(z)$, respectively. The symbols $\circ\!-\!\bullet$ and $\bullet\!-\!\circ$ denote forward and inverse Fourier- or z-transformation, respectively.

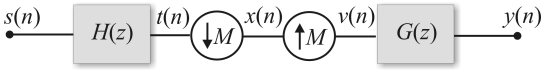

Fig. 1. One channel of a multirate filter bank.

II. Deterministic Signals

A. Decimation

Downsampling the filtered signal $t(n) \circ\!-\!\bullet T(z) = H(z)S(z)$ yields for the spectrum of the decimated signal $x(n)$ [36], [37]

$$X(z) = \frac{1}{M}\mathbf{s}_m^T(z^{1/M}) \cdot \mathbf{h}_m(z^{1/M}) \tag{1}$$

The energy spectrum is

$$\begin{aligned} R^E_{xx}(z) &= X(z)X(z^{-1}) \\ &= \frac{1}{M^2}\mathbf{s}_m^T(z^{1/M})\mathbf{h}_m(z^{1/M})\mathbf{h}_m^T(z^{-1/M})\mathbf{s}_m(z^{-1/M}) \end{aligned} \tag{2}$$

Shifting $s(n)$ by m samples to $s(n-m)$, $m = 0, \ldots, M-1$ multiplies $T(z)$ by z^{-m}. Since the energy spectrum of $x(n)$ generally depends on m, it is in the following denoted by $R^E_{xx}(m, z)$, and it obeys with Eq. (2)

$$\begin{aligned} R^E_{xx}(m,z) = \quad & \tfrac{1}{M} \sum_{k=0}^{M-1} T(z^{\frac{1}{M}}W^k) \cdot W^{-km} \cdot \\ & \tfrac{1}{M} \sum_{l=0}^{M-1} T(z^{-\frac{1}{M}}W^l) \cdot W^{-lm} \end{aligned} \tag{3}$$

Eq. (3) is the product of the m-th coefficients $i(m)$ and $j(m)$ of the inverse discrete Fourier transforms of $I(k) = T(z^{\frac{1}{M}}W^k)$ and $J(k) = T(z^{-\frac{1}{M}}W^k)$. With $i(m) \cdot j(m) \circ\!-\!\bullet$

$1/M \cdot I(k) * J(k)$, and grouping $R^E_{xx}(m,z)$, $m = 0,\ldots,M-1$, into a vector, we get

$$\left[R^E_{xx}(0,z), R^E_{xx}(1,z), \ldots, R^E_{xx}(M-1,z)\right]^T = \frac{\mathbf{W}^H}{M^2}\left[A_0(z^{1/M}), A_1(z^{1/M}), \ldots, A_{M-1}(z^{1/M})\right]^T \quad (4)$$

where $\mathbf{W}^H$ is the transjugated Fourier matrix, and $A_k(z)$ is the convolution of modulated DFT-spectra

$$A_k(z) = \sum_{l=0}^{M-1} T(zW^l)T(z^{-1}W^{k-l}) \quad (5)$$

Eq. (4) permits straightforward separation of the energy spectrum into shift-invariant and shift-variant parts. $R^E_{xx}(m,z)$ is shift-invariant, i.e., independent of m, if and only if $A_k(z) = 0$ for $k = 1,\ldots,M-1$. This is equivalent to the absence of aliasing. The energy spectrum is then equal to the average or shift-invariant part of Eq. (4) given by

$$\overline{R}^E_{xx}(z) = \frac{1}{M^2} A_0(z^{1/M}) \quad (6)$$

With aliasing, we define the shift-variant deviations $\Delta R^E_{xx}(m,z)$ from the shift-invariant part $\overline{R}^E_{xx}(z)$ by

$$\left[\Delta R^E_{xx}(0,z), \ldots, \Delta R^E_{xx}(M-1,z)\right]^T = \frac{\mathbf{W}^H}{M^2}\left[0, A_1(z^{1/M}), \ldots, A_{M-1}(z^{1/M})\right]^T \quad (7)$$

where $\Delta R^E_{xx}(m,z) = R^E_{xx}(m,z) - \overline{R}^E_{xx}(z)$.

B. Interpolation

Upsampling stretches the input signal $x(n)$ on the time axis, and correspondingly compresses its energy spectrum to $R^E_{vv}(z) = R^E_{xx}(z^M)$. The ACS of $x(n)$ is therefore upsampled like the signal $x(n)$ itself [38], [39]. Unlike decimation, interpolation introduces no shift dependencies into the energy spectrum. Upsampling of the shift-variant energy spectrum $R^E_{xx}(m,z^M)$ in Eq. (3) and filtering by $G(z)$ results in

$$R^E_{yy}(m,z) = G(z^{-1})R^E_{xx}(m,z^M)G(z) \quad . \quad (8)$$

Inserting Eq. (4) yields for the output energy spectra

$$\left[R^E_{yy}(0,z), \ldots, R^E_{yy}(M-1,z)\right]^T = \frac{\mathbf{W}^H}{M^2}\left[B_0(z), \ldots, B_{M-1}(z)\right]^T \quad (9)$$

where

$$B_k(z) = G(z^{-1})A_k(z)G(z) \quad (10)$$

As in Eq. (6), the shift-invariant part of the energy spectra is given by the average

$$\overline{R}^E_{yy}(z) = \frac{1}{M^2} B_0(z) \quad (11)$$

and the shift-variant deviations which remain after synthesis filtering are

$$\left[\Delta R^E_{yy}(0,z), \ldots, \Delta R^E_{yy}(M-1,z)\right]^T = \frac{\mathbf{W}^H}{M^2}\left[0, B_1(z), \ldots, B_{M-1}(z)\right]^T \quad (12)$$

C. Criteria for Shift Variance

Eqs. (9), (11) and (12) are the basis for our criteria assessing shift variance. We first develop a measure for the shift variance of the energy of $y(n)$. By integrating Eq. (9) over the unit circle, we obtain the shift-variant energies $E_{yy}(m)$

$$\left[E_{yy}(0), \ldots, E_{yy}(M-1)\right]^T = \mathbf{W}^H\left[e_0, e_1, \ldots, e_{M-1}\right]^T \quad (13)$$

where

$$E_{yy}(m) = \frac{1}{2\pi}\int_{-\pi}^{\pi} R^E_{yy}(m, e^{j\omega})d\omega \quad . \quad (14)$$

The energies e_k are given by

$$e_k = \frac{1}{2\pi M^2}\int_{-\pi}^{\pi} B_k(e^{j\omega})d\omega \quad (15)$$

where

$$B_k(e^{j\omega}) = \sum_{l=0}^{M-1} T(e^{j(\omega - \frac{2\pi l}{M})})T^*(e^{j(\omega + \frac{2\pi(k-l)}{M})})|G(e^{j\omega})|^2 \quad (16)$$

The shift-invariant part of the energy of $y(n)$ is then equivalent to the average $\overline{E}_{yy} = e_0$. The shift-variant energy deviations are

$$\left[\Delta E_{yy}(0), \ldots, \Delta E_{yy}(M-1)\right]^T = \mathbf{W}^H\left[0, e_1, \ldots, e_{M-1}\right]^T \quad (17)$$

with $\Delta E_{yy}(m) = E_{yy}(m) - \overline{E}_{yy}$. We assess the shift variance of signal energy by the normalized mean square energy deviation from the shift-invariant average. With Parseval's theorem for the DFT, this criterion becomes

$$C_e^2 = \frac{\frac{1}{M}\sum_{m=0}^{M-1}|\Delta E_{yy}(m)|^2}{(\overline{E}_{yy})^2} = \frac{\sum_{k=1}^{M-1}|e_k|^2}{|e_0|^2} \quad . \quad (18)$$

Evidently, the amount of shift variance generated depends on the anti-aliasing filter $H(z)$, while the anti-imaging filter $G(z)$ tends to attenuate the shift-variant components. If the bandwidth of $G(z)$ is sufficiently narrow (less than $2\pi/M$ if the anti-aliasing filter $H(z)$ does not prevent aliasing), shift variance in the output signal of the filter bank branch could even be eliminated. In PR filter banks, analysis and synthesis filters are, however, closely related. For instance, in orthogonal filter banks, filters are designed from a common lowpass FIR prototype $H(z)$ by modulation, time reversal and shifts. The bandwidths of $H(z)$ and $G(z)$ are then identical, since $|H(e^{j\omega})| = |G(e^{j\omega})|$. The energy spectrum of $y(n)$ is then always shift-variant.

The above criterion C_e^2 assesses the variance of signal energy over shift m, and, via the e_k, also provides information on which aliasing components are responsible for most of the variation. Changes in the shape of the energy spectrum, however, which do *not* result in a change of energy, escape evaluation by C_e^2. To devise an alternative criterion which captures all variations of the shape of the energy spectrum — including variations of signal energy — we interchange the order of integration and application of Parseval's theorem.

With

$$\sigma_e^2(e^{j\omega}) = \frac{1}{M}\sum_{m=0}^{M-1}|\Delta R_{yy}^E(m,e^{j\omega})|^2 = \frac{1}{M^4}\sum_{k=1}^{M-1}|B_k(e^{j\omega})|^2 \quad (19)$$

denoting the variance of the energy spectrum $R_{yy}^E(m,e^{j\omega})$ over m for each ω, a frequency-resolved criterion of the relative variation of the energy spectrum can be obtained by the normalization

$$\sigma_{eN}^2(e^{j\omega}) = \frac{\sigma_e^2(e^{j\omega})}{|\overline{R}^E(e^{j\omega})|^2} = \frac{\sum_{k=1}^{M-1}|B_k(e^{j\omega})|^2}{|B_0(e^{j\omega})|^2} \quad . \quad (20)$$

This expression is defined for all ω with $|B_0(e^{j\omega})| > 0$. Since the energy spectra are non-negative, $|B_0(e^{j\omega})| = 0$ for some frequency ω implies that the numerator of Eq. (20) is zero as well, which we take into account by setting $\sigma_{eN}^2(e^{j\omega}) = 0$ for these frequencies. Finally, averaging over ω yields the criterion

$$L_e^2 = \frac{1}{2\pi}\int_{-\pi}^{\pi}\sigma_{eN}^2(e^{j\omega})d\omega = \frac{1}{2\pi}\int_{-\pi}^{\pi}\frac{\sum_{k=1}^{M-1}|B_k(e^{j\omega})|^2}{|B_0(e^{j\omega})|^2}d\omega \quad (21)$$

Unlike the criterion C_e^2 above, this measure also captures changes in the energy spectra which do not result in a change of energy. Finally note that both criteria can equally be applied to assess the degree of shift variance in the subbands after analysis filtering and downsampling by replacing the power spectra in C_e^2 and L_e^2 with those derived in section II-A.

III. WSS Random Signals

A. Decimation

Decimation adds aliased components to the original power spectrum, but leaves the signal WSS. The power spectrum of the downsampled signal obeys (see, e.g., [32, Eq. (2)], or [39, Section 2.2])

$$R_{xx}(z) = \frac{1}{M}\cdot\sum_{k=0}^{M-1}H(z^{-1/M}W^{-k})\cdot R_{ss}(z^{1/M}W^k)H(z^{1/M}W^k) \quad . \quad (22)$$

B. Interpolation

Upsampling and synthesis filtering generally causes a WSS signal to become WSCS [23], [25], [27], [31]. The ACS $r_{yy}(m,n) = E[y(m)y(m+n)]$ then depends periodically on the reference position m with period M. Consequently, the power spectrum $R_{yy}(m,z)$ — defined as the z-transform of $r_{yy}(m,n)$ with respect to the lag parameter n — also depends on the position m [1]. Arranging the power spectra $R_{yy}(m,z)$ for $m = 0,\ldots,M-1$ into a vector, it is shown in the appendix that

$$[R_{yy}(0,z),\ldots,R_{yy}(M-1,z)]^T = \frac{R_{xx}(z^M)}{M}\mathbf{W}G(z)\mathbf{g}_m(z^{-1}) \quad (23)$$

holds. The average power spectrum is

$$\frac{1}{M}\sum_{m=0}^{M-1}R_{yy}(m,z) = \frac{R_{xx}(z^M)}{M}G(z)G(z^{-1}) \quad . \quad (24)$$

The nonstationary differences $\Delta R_{yy}(m,z)$ to the average spectrum are

$$[\Delta R_{yy}(0,z),\ldots,\Delta R_{yy}(M-1,z)]^T = \frac{R_{xx}(z^M)}{M}\mathbf{W}G(z)\left[0,G(z^{-1}W),\ldots,G(z^{-1}W^{M-1})\right]^T \quad (25)$$

These vanish for ideal anti-imaging filtering.

C. Criteria for Cyclostationarity

To quantify the cyclic nonstationarities of $y(n)$, we calculate the periodically varying power $P_y(m)$ by integrating Eq. (23) over the unit circle. The left-hand side yields

$$P_y(m) = \frac{1}{2\pi}\int_{-\pi}^{\pi}R_{yy}(m,e^{j\omega})d\omega \;, \quad m = 0,\ldots,M-1 \quad (26)$$

With the power p_n from the overlap of $G(z)$ and $G(z^{-1}W^n)$ defined as

$$p_n = \frac{1}{2\pi M}\int_{-\pi}^{\pi}R_{xx}(e^{j\omega M})G(e^{j\omega})G(e^{-j(\omega+2\pi n/M)})d\omega \quad , \quad (27)$$

where, from Eq. (22),

$$R_{xx}(e^{j\omega M}) = \frac{1}{M}\sum_{k=0}^{M-1}R_{ss}(e^{j(\omega-\frac{2\pi k}{M})})|H(e^{j(\omega-\frac{2\pi k}{M})})|^2 \quad , \quad (28)$$

we obtain with Eq. (23)

$$[P_y(0),\ldots,P_y(M-1)]^T = \mathbf{W}[p_0,\ldots p_{M-1}]^T \quad (29)$$

The stationary power average $\overline{P}_y$ then is

$$\overline{P}_y = \frac{1}{M}\sum_{m=0}^{M-1}P_y(m) = p_0 \quad (30)$$

and the nonstationary deviations $\Delta P_y(m)$ from the mean are

$$[\Delta P_y(0),\ldots,\Delta P_y(M-1)]^T = \mathbf{W}[0,p_1,\ldots,p_{M-1}]^T \quad (31)$$

To quantify the resulting cyclic nonstationarity, we define the normalized mean square power deviation from the average power as

$$C_p^2 = \frac{\frac{1}{M}\sum_{m=0}^{M-1}|\Delta P_y(m)|^2}{\left(\frac{1}{M}\sum_{m=0}^{M-1}P_y(m)\right)^2} = \frac{\sum_{n=1}^{M-1}|p_n|^2}{p_0^2} \quad (32)$$

In comparison to shift variance of deterministic signals, analysis and synthesis filters have now exchanged their roles:

[1] In, e.g., [40, Eq. (2)], the spectrum of the time-varying ACS with respect to the time lag is called the *instantaneous probabilistic spectrum*. As we will later on use $R_{yy}(m,z)$ to compute the periodically time-varying power, we continue to refer to it as power spectrum. For an interpretation of this quantity in terms of the Wiener-Khinchin theorem, see [40, p. 289].

the amount of nonstationarity generated depends on the anti-imaging filter $G(z)$, while the anti-aliasing filter $H(z)$ tends to attenuate the nonstationary components caused by an insufficiently narrow anti-imaging filter. As is evident from Eq. (23), if $G(z)$ eliminates all frequency images, $y(n)$ is again WSS [23], [31]. In channels of PR multirate filter banks with FIR filters, the channel output signals are always nonstationary.

The above criterion is the counterpart of the shift variance criterion C_e^2 in Eq. (18) for deterministic signals, and evaluates the periodic variations of the power of $y(n)$, but not variations of the shape of $R_{yy}(m,z)$ which do not lead to a change in power. To capture also changes in power spectra which do not result in a change of signal power we first apply Parseval's theorem to Eq. (25) and integrate then over frequency. For the left-hand side of Eq. (25), this leads to

$$\sigma_p^2(m) = \frac{1}{2\pi}\int_{-\pi}^{\pi} |\Delta R_{yy}(m,e^{j\omega})|^2 d\omega \tag{33}$$

which can be viewed as the energy of $\Delta R_{yy}(m,e^{j\omega})$ for a given m. From the right-hand side of Eq. (25), we obtain

$$D_p^2(k) = \frac{1}{2\pi}\int_{-\pi}^{\pi} |C_k(e^{j\omega})|^2 d\omega \tag{34}$$

where

$$C_k(z) = \frac{R_{xx}(z^M)}{M} G(z) G(z^{-1}W^k) \tag{35}$$

The energy average over $m = 0,\ldots,M-1$ then is

$$\frac{1}{M}\sum_{m=0}^{M-1}\sigma_p^2(m) = \sum_{k=1}^{M-1} D_p^2(k) \tag{36}$$

Normalizing by the energy of the average spectrum

$$\mu_p^2 = \frac{1}{2\pi}\int_{-\pi}^{\pi} |\overline{R}_{yy}(e^{j\omega})|^2 d\omega \tag{37}$$

leads to the normalized criterion

$$K_p^2 = \frac{\frac{1}{M}\sum_{m=0}^{M-1}\sigma_p^2(m)}{\mu_p^2} = \frac{\sum_{k=1}^{M-1} D_p^2(k)}{D_p^2(0)} \tag{38}$$

Note that this criterion is not fully analog to L_e^2 in Eq. (21): in Eq. (21), we first normalized to $|B_0(e^{j\omega})|^2$ and integrated only then over ω, whereas in Eq. (38), numerator and denominator are separately integrated over ω. The reason for this is that, since the cyclostationary ACS $r_{yy}(m,n)$ is formed from crosscorrelation sequences according to Eq. (56), $C_0(e^{j\omega})$ may vanish for some ω, while one or more of the $C_k(e^{j\omega})$ with $k = 1,\ldots,M-1$ do not. In contrast to this, $D_p^2(0)$ is always larger than zero (unless the signal $y(n)$ vanishes), so that Eq. (38) always exists.

Invoking Parseval's theorem, Eq. (38) can also be written in terms of the ACS $r_{yy}(m,n)$ as

$$K_p^2 = \frac{\frac{1}{M}\sum_{m=0}^{M-1}\sum_{n=-\infty}^{\infty}|r_{yy}(m,n)-\overline{r}_{yy}(n)|^2}{\sum_{n=-\infty}^{\infty}|\overline{r}_{yy}(n)|^2} \tag{39}$$

where $\overline{r}_{yy}(n) = 1/M\sum_{m=0}^{M-1} r_{yy}(m,n)$ is the average ACS. This shows that Eq. (38) can be viewed as a discrete-time version of the so-called degree-of-cyclostationarity (DCS) measure introduced by Zivanovic and Gardner in [40, Eq. (16)], which was defined for continuous-time cyclostationary signals and a symmetrically defined ACS. Eq. (38) can thus be regarded as evaluating the distance of the cyclostationary ACS $r_{yy}(m,n)$ to the nearest stationary ACS, or, equivalently, as the distance of the cyclostationary power spectrum $R_{yy}(m,e^{j\omega})$ to the closest stationary power spectrum. For the type of distance used, the closest stationary ACS and the closest stationary power spectrum are those of the stationary process obtained from the cyclostationary one by phase randomization [41], [42], and are given by the time averages $\overline{r}_{yy}(n)$ and $\overline{R}_{yy}(e^{j\omega})$, respectively [43, p. 373],[40]. In a similar manner, we may rewrite Eq. (32) in the time domain to

$$C_p^2 = \frac{\frac{1}{M}\sum_{m=0}^{M-1}|r_{yy}(m,0)-\overline{r}_{yy}(0)|^2}{\overline{r}_{yy}^2(0)} \tag{40}$$

In terms of the ACS $r_{yy}(m,n)$, the criterion C_p^2 thus assesses only the periodic changes of $r_{yy}(m,0)$ over m rather than those of the entire ACS. A comparable observation with respect to $r_{yy}^E(m,0)$ can be made for the shift variance criterion of C_e^2 in Eq. (18). Although the most appropriate criteria to assess shift variance and cyclostationarity may depend on the application, the criteria L_e^2 in Eq. (21) and K_p^2 in Eq. (38) are generally more comprehensive than C_e^2 and C_p^2, respectively. Based on the latter criteria, however, a relation can be derived between shift variance and cyclostationarity, as we will show in the next section.

IV. Flat-Spectrum Signals: A Duality

We have seen that for deterministic signals, shift variance is caused by decimation and thus mainly determined by the properties of the anti-aliasing filter $H(z)$. Conversely, for WSS signals, WS cyclostationarity is introduced by interpolation, thus being mainly determined by the anti-imaging filter $G(z)$. The structures of the expressions which describe shift variance of the signal energy in Eq. (18) and cyclostationarity in Eq. (32) are very similar: shift variance is introduced by the energies e_k, $k = 1,\ldots,M-1$, in Eqs. (15) and (16). Cyclostationarity is captured by the filter-overlap powers p_k in Eqs. (27) and (28). Though shift variance and cyclostationarity are different phenomena, they are closely related. We illustrate this by comparing the behavior of a deterministic unit impulse and WSS white noise. In the deterministic case with $s(n) = \delta(n)$, we have $S(z) = 1$ and $T(z) = H(z)$, whereas for the WSS case, we have $r_{ss}(n) = \delta(n)$ and $R_{ss}(z) = 1$. Eqs. (15) and (16) then simplify to

$$\begin{aligned} e_k &= \frac{1}{2\pi M^2}\sum_{l=0}^{M-1}\int_{-\pi}^{\pi}\left|G(e^{j\omega})\right|^2 \cdot \\ &\quad H(e^{j(\omega-\frac{2\pi l}{M})})H^*(e^{j(\omega+\frac{2\pi(k-l)}{M})})d\omega \end{aligned} \tag{41}$$

For the WSS signal, Eqs. (27) and (28) to calculate p_k become

$$\begin{aligned} p_k &= \frac{1}{2\pi M^2}\sum_{l=0}^{M-1}\int_{-\pi}^{\pi}\left|H(e^{j(\omega+\frac{2\pi l}{M})})\right|^2 \cdot \\ &\quad G(e^{j\omega})G^*(e^{j(\omega+\frac{2\pi k}{M})})d\omega \end{aligned} \tag{42}$$

where, in Eq. (28), $\omega - 2\pi l/M$ was replaced by $\omega + 2\pi l/M$, which changes only the order of the summation. After rotating each integrand by $2\pi l/M$ by the substitution $\tilde{\omega} = \omega + 2\pi l/M$, we obtain for p_k

$$p_k = \frac{1}{2\pi M^2} \sum_{l=0}^{M-1} \int_{-\pi}^{\pi} \left| H(e^{j(\tilde{\omega})}) \right|^2 \cdot G(e^{j(\tilde{\omega} - \frac{2\pi l}{M})}) G^*(e^{j(\tilde{\omega} + \frac{2\pi (k-l)}{M})}) d\tilde{\omega} \ . \quad (43)$$

This expression is identical to Eq. (41) for e_k, except that the analysis filter $H(z)$ and the synthesis filter $G(z)$ exchanged their places.

A. Paraunitary Filter Banks

Let us denote the filters in the i-th channel by $H_i(z)$ and $G_i(z)$. For the i-th channel, $i = 0, \ldots, M-1$, Eq. (41) becomes

$$e_k(i) = \frac{1}{2\pi M^2} \sum_{l=0}^{M-1} \int_{-\pi}^{\pi} J_{k,i}(l, e^{j\omega}) d\omega \quad (44)$$

where the l-th integrand is given by

$$J_{k,i}(l, z) = G_i(z) G_i(z^{-1}) H_i(zW^l) H_i(z^{-1} W^{k-l}) \quad (45)$$

In a similar manner, Eq. (43) becomes

$$p_k(i) = \frac{1}{2\pi M^2} \sum_{l=0}^{M-1} \int_{-\pi}^{\pi} I_{k,i}(l, e^{j\omega}) d\omega \quad (46)$$

with

$$I_{k,i}(l, z) = H_i(z) H_i(z^{-1}) G_i(zW^l) G_i(z^{-1} W^{k-l}) \quad (47)$$

In a paraunitary FIR filter bank, the synthesis filters are time-reversed versions of the analysis filters, since $G_i(z) = Mz^{-(L-1)} H_i(z^{-1})$, where L is the number of filter coefficients. Therefore,

$$\begin{aligned} J_{k,i}(l, z) &= W^{k(L-1)} I_{*k,i}(l, z^{-1}) \\ J_{k,i}(l, e^{j\omega}) &= e^{-j\omega k(L-1)} I^*_{k,i}(l, e^{j\omega}) \end{aligned} \quad (48)$$

where the subscript asterisk denotes complex conjugation of the coefficients of a function. This relationship between $J_{k,i}(l, z)$ and $I_{k,i}(l, z)$ reflects the time reversal and shifts. The absolute values of e_k and p_k are thus identical, and the criteria for shift variance and cyclostationarity take the same values:

$$|p_k(i)| = |e_k(i)| \Rightarrow C_p^2(i) = C_e^2(i) \quad (49)$$

B. Biorthogonal Filter Banks

In a two-channel birthogonal filter bank, the synthesis filter of channel 0 is related to the analysis filter of channel 1 and vice versa [37], [44], i.e. $G_0(z) = 2H_1(-z)$ and $G_1(z) = -2H_0(-z)$. Consequently, we obtain the cross relationships $|e_1(0)| = |p_1(1)|$ and $|e_1(1)| = |p_1(0)|$, yielding

$$C_p^2(1) = C_e^2(0) \ , \quad C_p^2(0) = C_e^2(1) \ . \quad (50)$$

The shift variance as evaluated by $C_e^2(0)$ in the lowpass channel is thus equal to the cyclic nonstationarity generated in the highpass channel as evaluated by $C_p^2(1)$, and vice versa.

V. Results

To apply our criteria to the evaluation of different filter banks, we reformulate them using the DFT. In the following, all DFTs are taken with length N (here: $N = 128$), which should be an integer multiple of M, where appropriate zero padding is applied. The discrete-time Fourier transform (DTFT) $H(e^{j\omega})$ of $h(n)$ is replaced by the DFT $H(k)$, and $H^*(e^{j\omega})$ by $H(N-k) = H^*(k)$. The modulated filter DTFT $H(e^{j(\omega - \frac{2\pi k}{M})})$ is translated according to

$$H(e^{j(\omega - \frac{2\pi k}{M})}) \bullet\!\!-\!\!\circ h(n) e^{j\frac{2\pi \frac{N}{M} kn}{N}} \circ\!\!-\!\!\bullet H\left[\left(q - \frac{N}{M}k\right)_N\right] \quad (51)$$

with $q = 0, \ldots, N-1$, and where the subscript N indicates that the corresponding arguments are taken modulo N. Replacing the DTFT versions of our criteria by their DFT counterparts is now straightforward.

We first evaluate shift variance and cyclic nonstationarity using the criteria C_e^2 and C_p^2, respectively. Table I shows the results for paraunitary two-channel filter banks with input $s(n) = \delta(n)$ in the deterministic case, and white noise (i.e., $r_{ss}(n) = \delta(n)$) in the WSS random case. As derived in section IV-A, results for shift variance and nonstationarity are then identical, and are therefore both given in Table I. To allow a direct comparison of the energies e_k and powers p_k, the coefficient sum of each lowpass prototype was normalized to one; this does not affect C_e^2 and C_p^2. The first two rows (john16, john8) refer to the Johnston filters of lengths 16 and 8, respectively. These are linear-phase quadrature mirror filters with approximate PR properties [45], [36]. The next two rows (prcqf16, prcqf8) denote the PR-conjugated quadrature filters by Smith and Barnwell, which are not linear phase, but provide PR [46], [47], [36]. The filter denoted by sha03 is the wavelet filter of length 8 developed specifically for low shift variance in [21] (coefficients: 0.0073, 0.015, -0.1197, 0.0698, 0.7196, 0.6711, 0.0999, -0.0488). The last row contains the Haar filter. Input energy and power are divided equally between both channels, therefore, $|e_0| = |p_0| = 0.5$ for each channel. For the prcqf-filters, the longer impulse response of the prcqf16 filter results in lower values of $|e_1|$ and $|p_1|$ and correspondingly lower shift variance and nonstationarity than the prcqf8 filter does. Shift variance and nonstationarity values for the sha03-filter are even lower. For the Johnston filters as well as for the Haar filter, the measures C_e^2 and C_p^2 both vanish, therefore, a shift of the input signal does not result in a change of *energy* of the output signal $y(n)$ of each filter bank channel. Similarly, if the input is white noise, the *power* of $y(n)$ is position independent. As discussed in sections II-C and III-C, this does not necessarily imply that the energy spectrum is shift invariant or that the correlation structure is position independent. Vanishing of C_e^2 despite non-ideal filtering is perhaps easiest explained for the Haar filter: the impulse response of the lowpass prototype and the absolute impulse response of the highpass filter are both constant. A shift of a single impulse at the input has thus no influence on subband energy.

Table II shows energies $|e_k(i)|$ and shift variance criteria $C_e^2(i)$ for both channels of the biorthogonal filters of lengths

filter, subband	$\|e_0\|$, $\|p_0\|$	$\|e_1\|$, $\|p_1\|$	C_e^2, C_p^2
john16	0.5	0	0
john8	0.5	0	0
prcqf16	0.5	0.0702	0.0197
prcqf8	0.5	0.1317	0.0693
sha03	0.5	0.0422	0.0071
Haar	0.5	0	0

TABLE I

ENERGIES $|e_k|$, POWERS $|p_k|$, BOTH FOR $k = 0, 1$, AND CRITERIA C_e^2, C_p^2 FOR PARAUNITARY TWO-CHANNEL FILTER BANKS. THE DETERMINISTIC INPUT SIGNAL WAS $s(n) = \delta(n)$, AND THE ACF OF THE WSS RANDOM INPUT SIGNAL $r_{ss}(n) = \delta(n)$. ALL VALUES ARE IDENTICAL FOR BOTH CHANNELS OF EACH FILTER BANK.

filter	C_e^2	C_p^2
john16	0	0
john8	0	0
prcqf16	0.0266	0.0196
prcqf8	0.0942	0.0589
M-PRQMF4	0.2702	0.1461
M-PRQMF6	0.0026	0.0016
M-PRQMF8	0	0
sha03	0.0132	0.0046
Haar	0	0
bior9/7	0.1283	0.1271
bior6/10	0	0
bior5/3	0.2477	0.2139

TABLE III

C_e^2 AND C_p^2 FOR PARAUNITARY AND BIORTHOGONAL TWO-CHANNEL FILTER BANKS AVERAGED OVER BOTH CHANNELS. FOR THE INPUT SIGNALS SEE TEXT.

9/7, 6/10, and 5/3, and $s(n) = \delta(n)$. In addition, the averages over both channels are provided. For the 9/7 and 5/3 filters, the energy $|e_1|$ is larger for the lowpass channel ($i = 0$) than for the highpass channel, generating a correspondingly higher shift variance. For the 6/10 filters, shift variance of energy practically vanishes, this is consistent with the observations made in [4], [48] with respect to the low shift variance of these filters. For a cyclostationarity analysis of these filters based on white noise as input, the values of $|p_k(i)|$ and $C_p^2(i)$ are identical to those of $|e_k(i)|$ and $C_e^2(i)$ in Table II with subband indices interchanged, as derived in section IV-B.

filter, subband	$\|e_0(i)\|$	$\|e_1(i)\|$	$C_e^2(i)$
bior9/7, $i = 0$	0.5041	0.2070	0.1686
$i = 1$	0.5041	0.1557	0.0954
avg.	0.5041	0.1813	0.132
bior6/10, $i = 0$	0.5033	0	0
$i = 1$	0.5033	0	0
avg.	0.5033	0	0
bior5/3, $i = 0$	0.5078	0.2891	0.3240
$i = 1$	0.5078	0.2109	0.1725
avg.	0.5078	0.2500	0.2483

TABLE II

ENERGIES $|e_k|$ FOR $k = 0, 1$, AND CRITERION $C_e^2(i)$ FOR BOTH CHANNELS OF BIORTHOGONAL TWO-CHANNEL FILTER BANKS WITH INPUT $s(n) = \delta(n)$.

Table III shows the values of C_e^2 and C_p^2 averaged over both channels of various two-channel filter banks. The deterministic input signal was a double-sided exponential impulse with energy spectrum equal to the power spectrum of a first-order autoregressive (AR(1)) WSS random signal with correlation coefficient $\rho = 0.9$, and the WSS input was an AR(1) random signal with $\rho = 0.9$. M-PRQMF4, -6, and -8 denote the multiplierless PR quadrature mirror filters of lengths 4, 6, and 8, respectively; their coefficients can be found in [36]. Table IV gives the results for each subband of the 8-channel DCT, MLT, and LOT with these input signals. The basis functions of the LOT are calculated from an eigensystem analysis of a Toeplitz covariance matrix with $\rho = 0.9$ [49, Chapter 1],[20, p.32]. Due to their longer basis functions, the MLT and LOT perform better than the DCT, with the LOT — the basis functions of which are specifically matched to the AR(1)-process — performing best.

The results given so far capture changes only variations in energy and power, respectively. Table V lists the values of the shift variance criterion L_e^2, which also captures changes in the shape of the energy spectrum, for both channels of the two-channel filter banks. Since in image data shift variance is visually most critical at fine detail structures such as lines and edges, the input signal here is $s(n) = \mathrm{sgn}(n) \cdot \exp\{-0.9|n|\}$, where $\mathrm{sgn}(n) = 1$ for $n \geq 0$, and $\mathrm{sgn}(n) = -1$ for $n < 0$. This is a double-sided exponential impulse with a sign change at the origin, which can be regarded as the gray level profile across an edge. The Haar filter now performs poorest, as expected, while the prcqf16 filters exhibit lowest shift variance. Among the linear phase filters, the biorthogonal 9/7 filters now perform best; in fact, they leave the biorthogonal 6/10 filters - which led the field in Table III - far behind. The sha03-filter is now also relatively weak. Among the M-PRQM-filters, the filters of length 4 outperform the others. To learn which spectral components contribute strongest to shift variance, Figure 2 shows the average of the normalized variance $\sigma_{eN}^2(e^{j\omega})$ in Eq. (20) over both filter bank channels of the Haar-, biorthogonal 9/7-, biorthogonal 6/10- and the M-PRQMF4 filters. Evidently, the area under the variance average is largest for the Haar filters. While for the M-PRQMF4 filters, the bandwidth of the averaged variance is comparable to that one of the Haar filters, the maximum value is only about a third of that of the Haar filters, thus explaining the lower value for L_e^2 in Table V. For the longer biorthogonal filters, the bandwidths of the variance averages are correspondingly narrower, with the biorthogonal 9/7 filters reaching only a maximum of about 0.12, thus explaining their low value for L_e^2 in Table V.

Table VI lists the values of $L_e^2(i)$ for all eight channels of DCT, MLT, and LOT driven by the same input signal. The DCT is still weakest, but the performance of the MLT is now rated better than that of the LOT.

We conclude our evaluations by an analysis of the nonstationarity introduced into an AR(1)-random process ($\rho = 0.9$), as captured by the criterion K_p^2. This criterion assesses the cyclic nonstationarity of the power spectrum, i.e, of the entire correlation structure, rather than only of the power. The results are listed in Tables VII and VIII. For the two-channel filter

	$C_e^2(0)$	$C_e^2(1)$	$C_e^2(2)$	$C_e^2(3)$	$C_e^2(4)$	$C_e^2(5)$	$C_e^2(6)$	$C_e^2(7)$	avg.
DCT	0.0028	0.3359	0.6884	0.5233	0.0809	0.6444	0.5508	0.5038	0.4163
MLT	0.0069	0.3906	0.2678	0.3291	0.4177	0.2609	0.2478	0.1297	0.2563
LOT	0.0063	0.3029	0.3066	0.0702	0.0816	0.1414	0.2518	0.075	0.1545
	$C_p^2(0)$	$C_p^2(1)$	$C_p^2(2)$	$C_p^2(3)$	$C_p^2(4)$	$C_p^2(5)$	$C_p^2(6)$	$C_p^2(7)$	avg.
DCT	0	0.5	0.5	0.5	0	0.5	0.5	0.5	0.3750
MLT	0.0238	0.2664	0.2578	0.3515	0.3976	0.2507	0.2502	0.1274	0.2407
LOT	0.0185	0.1854	0.2614	0.0637	0.1042	0.2396	0.2495	0.0552	0.1472

TABLE IV

UPPER HALF: SHIFT VARIANCE MEASURE $C_e^2(i)$ FOR EACH CHANNEL OF DCT, MLT, AND LOT. LOWER HALF: NONSTATIONARITY MEASURES $C_p^2(i)$ FOR THESE TRANSFORMS. THE LAST COLUMN LISTS THE AVERAGES.

	$L_e^2(0)$	$L_e^2(1)$	$L_e^2(2)$	$L_e^2(3)$	$L_e^2(4)$	$L_e^2(5)$	$L_e^2(6)$	$L_e^2(7)$	avg.
DCT	0.4463	0.5960	0.4434	0.4570	0.8253	0.4213	0.4961	0.4770	0.5203
MLT	0.1468	0.3770	0.3453	0.2162	0.1904	0.3227	0.3283	0.1655	0.2615
LOT	0.1969	0.5878	0.3858	0.5258	0.5298	0.3221	0.3712	0.1231	0.3803

TABLE VI

CRITERION $L_e^2(i)$ FOR ALL CHANNELS OF DCT, MLT, AND LOT, AND ITS AVERAGE OVER ALL CHANNELS.THE INPUT SIGNAL WAS A DOUBLE-SIDED EXPONENTIAL IMPULSE WITH A SIGN CHANGE AT THE ORIGIN.

filter	$L_e^2(0)$	$L_e^2(1)$	avg.
john16	0.1034	0.1277	0.1156
john8	0.1991	0.3017	0.2504
prcqf16	0.0060	0.0068	0.0064
prcqf8	0.1116	0.1520	0.1318
M-PRQMF4	0.1224	0.3071	0.2148
M-PRQMF6	0.2157	0.3215	0.2686
M-PRQMF8	0.2036	0.3222	0.2629
sha03	0.2291	0.3723	0.3007
Haar	0.3202	0.6720	0.4961
bior9/7	0.0267	0.0273	0.0270
bior6/10	0.2176	0.2383	0.2279
bior5/3	0.0351	0.0397	0.0374

TABLE V

CRITERION $L_e^2(i)$ FOR BOTH CHANNELS OF VARIOUS TWO-CHANNEL FILTER BANKS, AND ITS AVERAGE OVER BOTH CHANNELS. THE INPUT SIGNAL WAS A DOUBLE-SIDED EXPONENTIAL IMPULSE WITH A SIGN CHANGE AT THE ORIGIN.

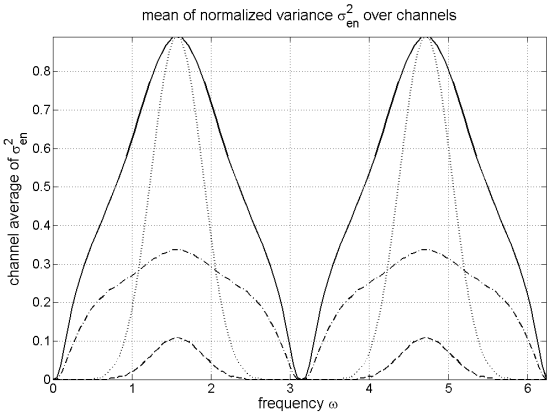

Fig. 2. Average of normalized variance $\sigma_{e_N}^2(e^{j\omega})$ over all subbands for the Haar filters (solid line), biorthogonal 9/7 filters (dashed line), biorthogonal 6/10 filters (dotted line), and the M-PRQMF4 filters (dash-dotted line), plotted for $0 \leq \omega < 2\pi$.

banks, the resulting nonstationarity is lowest for the prcqf16-filters, and strongest for the biorthogonal 5/3 filters. The biorthogonal 9/7 and 6/10 filters perform almost identically. The linear phase filters generating lowest nonstationarity are the john16-filters. Unlike in Table IV, the MLT is here slightly ahead of the LOT. Due to the higher downsampling ratio M, the eight-channel filter introduce more nonstationarity than the two-channel filter banks.

VI. CONCLUSIONS

We have analyzed the introduction of shift variance and the generation of cyclic nonstationarity in multirate filter banks in a parallel, comparative manner. We furthermore developed criteria for the quantitative asssessment of shift variance and nonstationarity. For shift variance, these criteria allow to separately assess the shift dependence of energy and of energy spectra. Similarly for nonstationarity, they allow to separately assess the nonstationary behavior of signal power and of power spectra or correlation structure. We also derived a duality between the shift-variant behavior of channel energy and the nonstationary behavior of channel power: For flat-spectrum signals in a paraunitary PR filter bank, the variations of channel energy and channel power as assessed by the criteria C_e^2 and C_p^2 are identical. Similarly for a biorthogonal filter bank, the shift variance measured in its lowpass channel is identical to the nonstationarity measured in its highpass channel, and vice versa. We have provided results for a variety of orthogonal and biorthogonal filter banks. With respect to filters such as the biorthogonal 6/10 filters, these results are consistent with observations in, e.g., [4], [48], where their low shift variance is highlighted. However, our results also show that considering channel energies or channel powers alone may provide an incomplete picture: for several filters including the Haar filters, channel energy is not shift variant and channel power is stationary for certain input signals, while energy spectrum and power spectrum vary considerably

	$K_p^2(0)$	$K_p^2(1)$	$K_p^2(2)$	$K_p^2(3)$	$K_p^2(4)$	$K_p^2(5)$	$K_p^2(6)$	$K_p^2(7)$	avg.
DCT	0.0574	1.3188	1.7589	1.7721	1.7803	1.6941	1.4695	0.6821	1.3166
MLT	0.0293	0.7016	0.7006	0.6997	0.6993	0.6990	0.6968	0.2794	0.5632
LOT	0.0389	0.7472	0.6843	0.7332	0.7079	0.8186	0.7875	0.3508	0.6085

TABLE VIII

NONSTATIONARITY CRITERION $K_p^2(i)$ FOR ALL CHANNELS OF DCT, MLT, AND LOT, AND ITS AVERAGE OVER ALL CHANNELS. THE INPUT SIGNAL WAS AN AR(1)-PROCESS.

filter	$K_p^2(0)$	$K_p^2(1)$	avg.
john16	0.0003	0.1426	0.0714
john8	0.0004	0.2887	0.1445
prcqf16	0.0002	0.1382	0.0692
prcqf8	0.0003	0.2450	0.1226
M-PRQMF4:	0.0020	0.3539	0.1780
M-PRQMF6:	0.0019	0.3110	0.1564
M-PRQMF8:	0.0002	0.2946	0.1474
sha03	0.0002	0.3059	0.1531
Haar	0.0047	0.3696	0.1872
bior9/7:	0.0001	0.3341	0.1671
bior6/10:	0.0001	0.3231	0.1616
bior5/3:	0.0003	0.4592	0.2297

TABLE VII

CRITERION $K_p^2(i)$ FOR BOTH CHANNELS OF VARIOUS TWO-CHANNEL FILTER BANKS, AND ITS AVERAGE OVER BOTH CHANNELS. THE INPUT SIGNAL WAS AN AR(1) RANDOM SIGNAL WITH $\rho = 0.9$.

over shift and position, respectively. We therefore believe that our criteria which quantify the variations of energy spectra and power spectra provide, for applications such as image filtering and compression, a more realistic view. When thus analyzing the shift variance of a test signal which can be regarded as representing the gray level profile across an edge in an image, the biorthogonal 9/7 filters outperformed the 6/10 filters by a wide margin, while the Haar filter fell to the bottom of the list, as expected. A similar observation holds for the introduction of nonstationarities: when examining channel powers only, as done in Table III, the biorthogonal 6/10 filters appear to outperform the 9/7 filters, while Table VII shows that when considering the power spectrum, both filters behave in a similar way. In all cases, our criteria take the properties of the input signals into account in terms of their energy spectra and power spectra. The evaluation can thus be carried out specifically for the signals where, e.g., shift variance is most critical, such as lines or edges in image data. This would allow to assess up to a certain degree the effects of, e.g., shift variance on the perceived subjective image quality, although no attempt was made to directly predict the visual image quality as in [50] for static images.

VII. APPENDIX

We provide two approaches to derive Eq. (23), viz. a direct one based on the polyphase decomposition of the interpolator [36], [37] shown in Fig. 3, and an alternative one using the effects of interpolation on cyclic correlation functions and cyclic spectral densities described in [29].

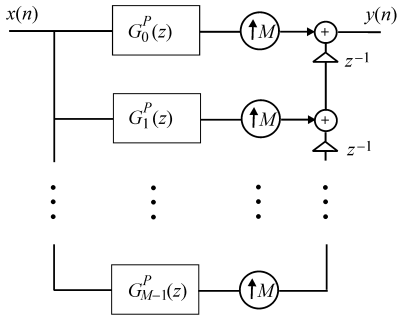

Fig. 3. Polyphase decomposition of the interpolator.

With the kth polyphase component $G_k^p(z)$ of $G(z)$ given by

$$G_k^p(z) = \sum_{n=-\infty}^{\infty} g(nM+k)z^{-n}\,, \quad k = 0, \ldots, M-1 \quad (52)$$

the filter $G(z)$ can be written as [51]

$$G(z) = \sum_{k=0}^{M-1} z^{-k} G_k^p(z^M) \quad (53)$$

Vice versa, the polyphase components depend on the modulation vector of $G(z)$ according to

$$\left[G_0^p(z), z^{-1/M}G_1^p(z), \ldots, z^{-(M-1)/M}G_{M-1}^p(z)\right]^T = \frac{\mathbf{W}}{M}\mathbf{g}_m(z^{1/M}) \quad (54)$$

As is evident from Fig. 3, the ACS $r_{yy}(m,n)$ corresponds to the crosscorrelation sequence between the outputs of two polyphase components of $G(z)$ [52]. Since $r_{yy}(m,n)$ depends periodically on m, we set $m = lM+i$, $i = 0, \ldots, M-1$, and calculate the ith power spectrum $R_{yy}(i,z)$ by the transform $r_{yy}(lM+i,n) \;\circ\!\!-\!\!\bullet\; R_{yy}(i,z)$. Its polyphase representation is

$$R_{yy}(i,z) = \sum_{k=0}^{M-1} z^{-k} R_{yyk}^p(i,z^M), \quad i,k = 0, \ldots, M-1 \quad (55)$$

The kth polyphase component $R_{yyk}^p(i,z)$ is the crosscorrelation of the outputs of $G_i^p(z)$ and $G^p_{(i+k)\text{mod } M}(z)$:

$$R_{yyk}^p(i,z) = R_{xx}(z) z^{\left\lfloor \frac{i+k}{M} \right\rfloor} G_i^p(z^{-1}) G^p_{(i+k)\text{mod } M}(z) \quad (56)$$

where $\lfloor x \rfloor$ is the floor of x. Since here

$$\left\lfloor \frac{i+k}{M} \right\rfloor M = i + k - (i+k)\text{mod } M \quad (57)$$

and with Eqs. (53) and (55), we obtain

$$R_{yy}(i,z) = R_{xx}(z^M) z^i G_i^p(z^{-M}) G(z) \tag{58}$$

Applying the ith component of Eq. (54) to the upsampled and mirrored polyphase component $G_i^p(z^{-M})$, and stacking the results for $i = 1, \ldots, M-1$ leads to Eq. (23).

Alternatively, we may start from the cyclic correlation function defined in [29, Eq. (21)], which, translated into our notation, reads

$$r_{yy}^c(m,n) = \frac{1}{M} \sum_{k=0}^{M-1} r_{yy}(k,n) W^{-mk} \tag{59}$$

The cyclic spectral density function $S_{yy}(m,z)$ [29, Eq. (22)] is defined as the transform of $r_{yy}^c(m,n)$ with respect to n, yielding

$$\begin{aligned} S_{yy}(m,z) &= \sum_{n=-\infty}^{\infty} r_{yy}^c(m,n) z^{-n} \\ &= \frac{1}{M} \sum_{k=0}^{M-1} W^{-mk} \sum_{n=-\infty}^{\infty} r_{yy}(k,n) z^{-n} \end{aligned} \tag{60}$$

Since $\sum_n r_{yy}(k,n) z^{-n} = R_{yy}(k,z)$, this can be written as

$$\begin{aligned} [S_{yy}(0,z), \ldots, S_{yy}(M-1,z)]^T &= \\ \frac{\mathbf{W}^H}{M} [R_{yy}(0,z), \ldots, R_{yy}(M-1,z)]^T & \end{aligned} \tag{61}$$

Vice versa, we obtain

$$\begin{aligned} [R_{yy}(0,z), \ldots, R_{yy}(M-1,z)]^T &= \\ \mathbf{W} [S_{yy}(0,z), \ldots, S_{yy}(M-1,z)]^T & \end{aligned} \tag{62}$$

As derived in [29, Eq. (36)], the cyclic spectral density of the interpolated signal obeys

$$S_{yy}(m,z) = \frac{1}{M} G(z) R_{xx}(z^M) G(z^{-1} W^m) \tag{63}$$

which, with Eq. (62), leads to Eq. (23).

REFERENCES

[1] R. E. Crochiere and L. R. Rabiner, "Interpolation and decimation of digital signals – a tutorial review," *Proceedings of the IEEE*, vol. 69, no. 3, pp. 300–331, 1981.

[2] ——, *Multirate Digital Signal Processing*. Englewood Cliffs: Prentice-Hall, 1983.

[3] E. P. Simoncelli, W. T. Freeman, E. H. Adelson, and D. J. Heeger, "Shiftable multiscale transforms," *IEEE Transactions on Information Theory*, vol. 38, no. 2, pp. 587–607, 1992.

[4] J. D. Villasenor, B. Belzer, and J. Liao, "Wavelet filter evaluation for image compression," *IEEE Transactions on Image Processing*, vol. 4, no. 8, pp. 1053–1060, 1995.

[5] M. Antonini, M. Barlaud, P. Mathieu, and I. Daubechies, "Image coding using wavelet transform," *IEEE Transactions on Image Processing*, vol. 1, no. 2, pp. 205–230, 1992.

[6] A. Skodras, C. Christopoulos, and T. Ebrahimi, "The JPEG 2000 still image compression standard," *IEEE Signal Processing Magazine*, vol. September, pp. 36–57, 2001.

[7] M. Stahl, T. Aach, and S. Dippel, "Digital radiography enhancement by nonlinear multiscale processing," *Medical Physics*, vol. 27, no. 1, pp. 56–65, 2000.

[8] C. M. Loeffler and C. S. Burrus, "Optimal design of periodically time-varying and multirate digital filters," *IEEE Transactions on Acoustics, Speech, and Signal Processing*, vol. 32, no. 5, pp. 991–997, 1984.

[9] P. P. Vaidyanathan and S. K. Mitra, "Polyphase networks, block digital filtering, LPTV systems, and alias-free QMF banks: A unified approach based on pseudocirculants," *IEEE Transactions on Acoustics, Speech, and Signal Processing*, vol. 36, pp. 381–391, 1988.

[10] H. Xiong, T. Zhang, and Y. S. Moon, "A translation- and scale invariant adaptive wavelet transform," *IEEE Transactions on Image Processing*, vol. 9, no. 12, pp. 2100–2108, 2000.

[11] J. Tian, "Comments on a translation- and scale-invariant adaptive wavelet transform," *IEEE Transactions on Image Processing*, vol. 12, no. 9, pp. 1091–1093, 2003.

[12] J. Fan and A. Laine, *Contrast Enhancement by Multiscale and Nonlinear Operators*. Boca Raton, FL: CRC Press, 1996, pp. 163–189.

[13] R. R. Coifman and D. L. Donoho, "Translation-invariant de-noising," in *Wavelets and Statistics*, A. Antoniades and G. Oppenheim, Eds. New York: Springer, 1995, pp. 125–150.

[14] J. Liang and T. W. Parks, "A translation-invariant wavelet representation with applications," *IEEE Transactions on Signal Processing*, vol. 44, no. 2, pp. 225–232, 1996.

[15] H. Malvar, "A modulated complex lapped transform and its application to audio processing," in *Proceedings ICASSP-99*. Phoenix, AZ: IEEE, March 15–19 1999, pp. 1421–1424.

[16] I. W. Selesnick, R. G. Baraniuk, and N. G. Kingsbury, "The dual-tree complex wavelet transform," *IEEE Signal Processing Magazine*, vol. November, pp. 123–151, 2005.

[17] N. Kingsbury, "Complex wavelets for shift-invariant analysis and filtering of signals," *Applied and Computational Harmonic Analysis*, vol. 10, pp. 234–253, 2001.

[18] D. Kunz and T. Aach, "Lapped directional transform: A new transform for spectral image analysis," in *Proceedings ICASSP-99*. Phoenix, AZ: IEEE, March 15–19 1999, pp. 3433–3436.

[19] T. Aach and D. Kunz, "A lapped directional transform for spectral image analysis and its application to restoration and enhancement," *Signal Processing*, vol. 80, no. 11, pp. 2347–2364, 2000.

[20] T. Aach, "Fourier, block and lapped transforms," in *Advances in Imaging and Electron Physics*, P. W. Hawkes, Ed., vol. 128. San Diego: Academic Press, 2003, pp. 1–52.

[21] L. K. Shark and C. Yu, "Design of shift-invariant orthonormal wavelet filter banks via genetic algorithm," *Signal Processing*, vol. 83, pp. 2579–2591, 2003.

[22] F. Mintzer and B. Liu, "Aliasing error in the design of multirate filters," *IEEE Transactions on Acoustics, Speech, and Signal Processing*, vol. 26, pp. 76–88, 1978.

[23] V. P. Sathe and P. P. Vaidyanathan, "Effects of multirate systems on the statistical properties of random signals," *IEEE Transactions on Signal Processing*, vol. 41, no. 1, pp. 131–146, 1993.

[24] A. K. Soman and P. P. Vaidyanathan, "Coding gain in paraunitary analysis/synthesis systems," *IEEE Transactions on Signal Processing*, vol. 41, no. 5, pp. 1824–1835, 1993.

[25] U. Petersohn, N. J. Fliege, and H. Unger, "Exact analysis of aliasing effects and non-stationary quantization noise in multirate systems," in *Proceedings IEEE International Conference on Acoustics, Speech, and Signal Processing (ICASSP)*. Adelaide: IEEE, May 1994, pp. III–173–III–176.

[26] U. Petersohn, H. Unger, and W. Wardenga, "Beschreibung von Multirate-Systemen mittels Matrixkalkül," *AEÜ - International Journal of Electronics and Communications*, vol. 48, no. 1, pp. 34–41, 1994.

[27] U. Petersohn, H. Unger, and N. J. Fliege, "Exact deterministic and stochastic analysis of multirate systems with application to fractional sampling rate conversion," in *IEEE International Symposium on Circuits and Systems (ISCAS94), Vol. 2*. Piscataway: IEEE, May 30 - June 2 1994, pp. 177–180.

[28] S. Ohno and H. Sakai, "Optimization of filter banks using cyclostationary spectral analysis," in *Proceedings IEEE International Conference on Acoustics, Speech, and Signal Processing (ICASSP)*. Detroit, MI: IEEE, May 1995, pp. 1292–1295.

[29] ——, "Optimization of filter banks using cyclostationary spectral analysis," *IEEE Transactions on Signal Processing*, vol. 44, no. 11, pp. 2718–2725, 1996.

[30] A. Mertins, *Signaltheorie*. Stuttgart: Teubner, 1996.

[31] S. Akkarakaran and P. P. Vaidyanathan, "Bifrequency and bispectrum maps: A new look at multirate systems with stochastic inputs," *IEEE Transactions on Signal Processing*, vol. 48, no. 3, pp. 723–736, 2000.

[32] A. N. Akansu and H. Caglar, "A measure of aliasing energy in multiresolution signal decomposition," in *Proceedings ICASSP-92*. San Francisco, CA: IEEE, March 23–26 1992, pp. VI–621–VI–624.

[33] L. Izzo and A. Napolitano, "Multirate processing of time series exhibiting higher order cyclostationarity," *IEEE Transactions on Signal Processing*, vol. 46, no. 2, pp. 429–439, 1998.
[34] B. Lal, S. D. Joshi, and R. K. P. Bhatt, "Second-order statistical characterization of the filter banks and its elements," *IEEE Transactions on Signal Processing*, vol. 47, no. 6, pp. 1745–1749, 1999.
[35] E. Serpedin, F. Panduru, I. Sari, and G. B. Giannakis, "Bibliography on cyclostationarity," *Signal Processing*, vol. 85, pp. 2233–2303, 2005.
[36] A. N. Akansu and R. A. Haddad, *Multiresolution Signal Decomposition*. Boston: Academic Press, 2001.
[37] G. Strang and T. Nguyen, *Wavelets and Filterbanks*. Wellesley, MA, USA: Wellesley-Cambridge Press, 1997.
[38] T. Aach, "Shift variance and cyclostationarity in multirate filter banks," in *6th Nordic Signal Processing Symposium (NORSIG)*. Meripuisto, Espoo: IEEE, ISBN: 951-22-7065-X (print), 951-22-7031-5 (CD-ROM), 951-22-7032-3 (Web, http://www.wooster.hut.fi/publications/norsig2004), June 9–11 2004, pp. 85–88.
[39] ——, "Quantitative comparison of shift variance and cyclostationarity in multirate filter banks," in *International Workshop on Spectral Methods and Multirate Signal Processing (SMMSP)*, T. Saramäki, K. Egiazarian, and J. Astola, Eds. Vienna: TICSP Series, ISBN: 952-15-1229-6 (print), 952-15-1241-5 (CD-ROM), Sept. 11 – 12 2004, pp. 7–14.
[40] G. D. Zivanovic and W. A. Gardner, "Degrees of cyclostationarity and their application to signal detection and estimation," *Signal Processing*, vol. 22, pp. 287–297, 1991.
[41] W. A. Gardner, "Stationarizable random processes," *IEEE Transactions on Information Theory*, vol. 24, no. 1, pp. 8–22, 1978.
[42] W. A. Gardner, A. Napolitano, and L. Paura, "Cyclostationarity: Half a century of research," *Signal Processing*, vol. 86, pp. 639–697, 2006.
[43] A. Papoulis, *Probability, Random Variables, and Stochastic Processes (3rd ed.)* New York: McGraw-Hill, 1991.
[44] J. R. Ohm, *Multimedia Communication Technology*. Berlin: Springer Verlag, 2003.
[45] J. D. Johnston, "A filter family designed for use in quadrature mirror filter banks," in *Proc. ICASSP 1980*. Piscataway: IEEE, 1980, pp. 291–294.
[46] M. J. T. Smith and T. P. Barnwell III, "A procedure for designing exact reconstruction filter banks for tree-structured subband coders," in *Proceedings IEEE International Conference on Acoustics, Speech, and Signal Processing (ICASSP)*. Denver: IEEE, March 1984, pp. 27.1.1–27.1.4.
[47] ——, "Exact reconstruction for tree-structured subband coders," *IEEE Transactions on Acoustics, Speech, and Signal Processing*, vol. 34, pp. 434–441, 1986.
[48] J. Zan, M. O. Ahmad, and M. N. S. Swamy, "Comparison of wavelets for multiresolution motion estimation," *IEEE Transactions on Circuits and Systems for Video Technology*, vol. 16, no. 3, pp. 439–446, 2006.
[49] H. S. Malvar, *Signal Processing with Lapped Transforms*. Norwood, MA: Artech House, 1992.
[50] Z. Wang and A. C. Bovik, "A universal image quality index," *IEEE Signal Processing Letters*, vol. 9, pp. 81–84, 2002.
[51] H. Johansson and O. Gustafsson, "Linear-Phase FIR Interpolation, Decimation and Mth-Band Filters Utilizing the Farrow Structure," *IEEE Transactions on Circuits and Systems–I:Regular Papers*, vol. 52, no. 10, pp. 2197–2207, 2005.
[52] T. Aach, "Shift variance in multiscale filtering," in *International Workshop on Spectral Methods and Multirate Signal Processing (SMMSP)*, T. Saramäki, K. Egiazarian, and J. Astola, Eds. Barcelona, Spain: TICSP Series, ISBN: 952-15-1062-5, September 13–14 2003, pp. 23–30.

Til Aach (M 1994 – SM 2002) received his diploma and Doctoral degrees, both in EE, from RWTH Aachen University in 1987 and 1993, respectively. While working towards his Doctoral Degree, he was a research scientist with the Institute for Communications Engineering, RWTH Aachen University, being in charge of several projects in image analysis, 3D-television and medical image processing. From 1993 to 1998, he was with Philips Research Labs, Aachen, Germany, where he was responsible for several projects in medical imaging, image processing and analysis. In 1996, he was also an independent lecturer with the University of Magdeburg, Germany. In 1998, he was appointed a Full Professor and Director of the Institute for Signal Processing, University of Luebeck. In 2004, he became Director of the Institute of Imaging and Computer Vision, RWTH Aachen University. His research interests are in medical and industrial image processing, signal processing, pattern recognition, and computer vision. He has authored or co-authored over 160 papers, and received several awards, among these the award of the German "Informationstechnische Gesellschaft" (ITG/VDE), for a paper published in the IEEE Transactions on Image Processing in 1998. Dr. Aach is named as a co-inventor in about 20 patents. He is an Associate Editor of the IEEE Transactions on Image Processing, and was Technical Program Co-Chair for the IEEE Southwest Symposium on Image Analysis and Interpretation (SSIAI) in 2000, 2002, 2004, and 2006. He is a member of the Bio-Imaging and Signal Processing Committee (BISP-TC) of the IEEE Signal Processing Society.